AGU PUBLICATIONS

Geophysical Research Letters

RESEARCH LETTER
10.1002/2015GL064355

Key Points:
- Ice shelf collapse reduces back pressure by up to 30% at the grounding line
- Ice shelf collapse causes instantaneous speedup that extends 15 km inland
- Hektoria, Green, and Crane speed up >100 m/yr, Flask and Leppard remain unaffected

Supporting Information:
- Supporting Information S1

Correspondence to:
J. De Rydt,
janryd69@bas.ac.uk

Citation:
De Rydt, J., G. H. Gudmundsson, H. Rott, and J. L. Bamber (2015), Modeling the instantaneous response of glaciers after the collapse of the Larsen B Ice Shelf, *Geophys. Res. Lett.*, *42*, 5355–5363, doi:10.1002/2015GL064355.

Received 27 APR 2015
Accepted 19 JUN 2015
Accepted article online 26 JUN 2015
Published online 7 JUL 2015

Modeling the instantaneous response of glaciers after the collapse of the Larsen B Ice Shelf

J. De Rydt[1], G. H. Gudmundsson[1], H. Rott[2,3], and J. L. Bamber[4]

[1]British Antarctic Survey, Cambridge, UK, [2]ENVEO IT GmbH, Innsbruck, Austria, [3]Institute for Meteorology and Geophysics, University of Innsbruck, Innsbruck, Austria, [4]Bristol Glaciology Centre, School of Geographical Sciences, University of Bristol, Bristol, UK

Abstract Following the disintegration of the Larsen B Ice Shelf, Antarctic Peninsula, in 2002, regular surveillance of its ~20 tributary glaciers has revealed a response which is varied and complex in both space and time. The major outlets have accelerated and thinned, smaller glaciers have shown little or no change, and glaciers flowing into the remnant Scar Inlet Ice Shelf have responded with delay. In this study we present the first areawide numerical analysis of glacier dynamics before and immediately after the collapse of the ice shelf, combining new data sets and a state-of-the-art numerical ice flow model. We simulate the loss of buttressing at the grounding line and find a good qualitative agreement between modeled changes in glacier flow and observations. Through this study, we seek to improve confidence in our numerical models and their ability to capture the complex mechanical coupling between floating ice shelves and grounded ice.

1. Introduction

In February 2002, most of the Larsen B Ice Shelf (LBIS) on the North East coast of the Antarctic Peninsula broke apart in less than a month. Despite the previous disintegration of smaller ice shelves around the Peninsula in response to a changing climate [*Rott et al.*, 1996; *Scambos et al.*, 2000; *Cook and Vaughan*, 2010], the rate and extent of the 2002 collapse was exceptional and the most dramatic observed so far. Good satellite coverage before, during, and after the disintegration, complemented by ground-based measurements, made this one of the best documented large-scale events in recent history of the cryosphere. Observations of surface velocities and elevation showed that glaciers previously feeding the ice shelf (Figure 1), accelerated and thinned [*Scambos et al.*, 2004; *Rignot et al.*, 2004; *Hulbe et al.*, 2008; *Rott et al.*, 2011; *Shuman et al.*, 2011], leading to an overall mass loss of about 8 Gt a^{-1} from 2001 to 2010 [*Scambos et al.*, 2014] and an increased discharge of grounded ice into the ocean, which is still ongoing today [*Berthier et al.*, 2012; *Wuite et al.*, 2015]. The acceleration, thinning, and associated grounding line retreat has been complex in behavior and highly variable in time and space, with some tributaries reacting rapidly, others with delay, and some hardly at all [*Scambos et al.*, 2014; *Wuite et al.*, 2015; *Khazendar et al.*, 2015]. Figure 1 shows the change in ice front position from 1995 to 2009, as well as the simultaneous speedup and grounding line retreat of the tributary glaciers.

Prior to this event, the mechanical coupling between ice shelves and their tributaries was subject to debate [*Hindmarsh and Le Meur*, 2001; *Ritz et al.*, 2001; *Vieli and Payne*, 2005], and the impact of changes to ice shelf thickness and extent on the upstream dynamics remained uncertain. The aftermath of the LBIS collapse unambiguously showed that the ice shelf acted as a natural barrier, providing buttressing (or back forces) that reduced the seaward motion of the grounded ice. Once the ice shelf collapsed, the reduction in back forces led to an acceleration of most tributary glaciers, a behavior that had previously been observed for tributary glaciers of the Larsen A Ice Shelf [*Rott et al.*, 2002]. The important role of ice shelves as stabilizing features has since been confirmed on a wider scale, as comprehensive studies using satellite measurements have shown enhanced coastal discharge in large regions of West Antarctica (in particular, the Amundsen Sea sector) and around the Antarctic Peninsula, associated with a consistent and accelerating decrease in extent and thickness of the ice shelves in those areas [*Pritchard et al.*, 2012; *Wouters et al.*, 2015].

During the period since the collapse of the LBIS, numerical ice flow models have become increasingly more advanced in describing the observed dynamical changes of the Antarctic Ice Sheet, and their performance has been evaluated in a series of benchmark tests [*Pattyn et al.*, 2012, 2013]. In particular, key physical processes

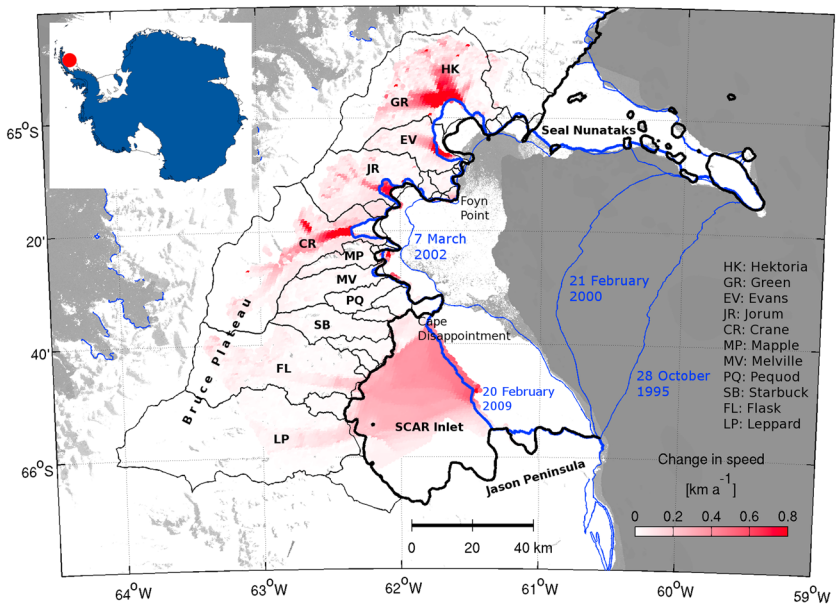

Figure 1. Overview of the study region, showing the Larsen B Embayment on the East Coast of the Antarctic Peninsula, overlain on a subset of the LIMA mosaic for Antarctica. The white-to-red color scale specifies the difference in surface speed between 2009 and 1995, obtained from satellite observations [*Wuite et al.*, 2015]. Blue lines indicate the ice front location for different times between 1995 and 2009; the thick black line delineates the 1995 grounding line location; thin black lines outline the drainage basins for the different tributaries [*Cook et al.*, 2014], and names of the most prominent glaciers are listed.

that control the coupling between the ice shelves and the grounded ice sheet, and the ability of numerical models to track the advance and retreat of the grounding line, have received special attention. However, previous modeling studies for the LBIS and wider Antarctic Peninsula did not incorporate these key processes, as they were either flow line approaches, studies that did not include a migrating grounding line or neglected the collapse of the ice shelves all together, or studies where the grounding line migration was directly prescribed [*Vieli et al.*, 2006, 2007; *Barrand et al.*, 2013, 2006; *Kulessa et al.*, 2014]. Results of these studies are expected to be incomplete, in particular, for glaciers that were previously buttressed by an ice shelf or glaciers that are flowing into ice shelves that are vulnerable to collapse.

The work presented here is a first step toward a more comprehensive treatment of dynamical changes on the Antarctic Peninsula in response to its retreating ice shelves. We use a state-of-the-art ice flow model and assimilate a number of new observational data sets for the Larsen B area, with three main goals: (1) to address the complicated spatial distribution of buttressing imposed by the ice shelf, (2) to understand the observed complex response of its glaciers to the loss of buttressing, and (3) to test the ability of our model to reproduce such complex behavior. To improve on existing flow line experiments [*Vieli et al.*, 2006, 2007], we solve the stress balance in two horizontal dimensions at a sufficiently high resolution (~500 m) for the entire Larsen B Embayment, including all its tributary glaciers. We use an adjoint inversion method to obtain important information about the englacial viscosity of the ice shelf before its collapse, and basal sliding properties of the narrow valley glaciers, using detailed observations of surface velocity and ice thickness. Results for a series of diagnostic perturbation experiments are presented, which simulate the disintegration of the ice shelf at various stages in time. Loss of the ice shelf leads to a reduction in back pressure at the grounding line of the main tributaries, and causes an immediate increase in their flow speed which extends more than 10 km upstream. Other smaller tributaries show little or no change, whereas Scar Inlet speeds up twofold, in line with observations.

2. Data Sets

This study was aided by the recent release of a detailed surface velocity map of the LBIS and all its tributary glaciers for the period late 1995 to early 1996, i.e., more than 6 years prior to the collapse of the ice shelf [*Wuite et al.*, 2015]. The study reanalyzed ERS1-2 repeat-pass Synthetic Aperture Radar data using interferometric

techniques to obtain a velocity map with complete coverage of the area at 50 m resolution. For the same time period, we use radar altimeter data from the ERS-1 geodetic phase to obtain the surface elevation of the ice shelf. The raw data were detided using the CATS model [*Padman et al.*, 2002], and corrections for the geoid and mean dynamic topography were applied. Results were cross-checked against data from the 1997–1998 British Antarctic Survey airborne radio echo sounder survey [*Holland et al.*, 2009], and a mean difference between the data sets of −0.87 m with a spread of about 1 m was obtained. The ice shelf thickness was computed from the surface elevation using a floatation criterion and a correction for the firn column air content obtained by *Holland et al.* [2011].

The surface elevation of the grounded ice was taken from the Antarctic Peninsula digital elevation model (API-DEM) by *Cook et al.* [2012], based on the ASTER GDEM. The latter is a mosaic of ASTER scenes with unspecified acquisition dates between 2000 and 2009 and therefore possibly contaminated by a thinning signal that has been observed for some glaciers after the collapse of the ice shelf in 2002 [*Rignot et al.*, 2004; *Rott et al.*, 2011; *Shuman et al.*, 2011; *Berthier et al.*, 2012]. In order to correct this uncertainty and to obtain a surface elevation that is closer to the (unobserved) precollapse values, we applied a correction to the API-DEM, requiring the ice upstream of the 1995 grounding line to be at or below floatation. The grounding line position was taken from the ERS InSAR analysis of *Rack et al.* [2000]. This correction raised the surface by up to 60 m for Crane Glacier (the geographical location and names of all glaciers are listed Figure 1) and up to 80 m for Hektoria-Green-Evans Glaciers over an area extending up to 5 km upstream of the grounding line. For Crane Glacier, the value is in line with detailed observations of surface drawdown after 2002 [*Scambos et al.*, 2011].

The bedrock elevation downstream of the grounding line was derived from all available multibeam and single beam bathymetric shiptrack data in the Larsen B Embayment, including a unique survey of the grounding line zones of Crane and Jorum Glaciers stretching several kilometers inland of their 1995 grounding line positions [*Rebesco et al.*, 2014]. For areas upstream of the grounding line (and without shipborne cover), we used the bedrock DEM derived by *Huss and Farinotti* [2014], which contains measurements from NASA's IceBridge mission as well as ground-based measurements. The bathymetric and inland bedrock data sets were joined by interpolation over a 4 km wide zone along the grounding line, except in areas where continuous shiptrack data across the grounding line were available. The resulting bedrock data set has several benefits compared to BEDMAP2 [*Fretwell et al.*, 2013], such as a higher resolution, better data coverage, and an improved representation of nunataks and rock outcrops.

3. Model Inversion

The breakup of the LBIS in February 2002 produced a stress perturbation which lead to profound dynamical changes and an imbalance of the remainder of the ice shelf and the upstream grounded ice [*Scambos et al.*, 2004; *Rott et al.*, 2011]. In order to simulate the abrupt change in forces and the repercussions on ice flow, the distribution of balanced stresses prior to the collapse of the ice shelf needs to be known. We used the precollapse (1995) observations of surface velocity, surface elevation, and ice thickness, described in section 2, to set up a state-of-the-art ice flow model, Úa, which has previously been used successfully to study ice shelf-ice stream systems both in idealized setups [*Gudmundsson et al.*, 2012; *Pattyn et al.*, 2013; *Gudmundsson*, 2013] as well as in realistic cases with a complicated geometry [*Favier et al.*, 2014].

The numerical model, Úa, solves the ice dynamics equations in the shallow ice stream approximation (SSTREAM or SSA) [see, e.g., *Hutter*, 1983; *MacAyeal*, 1989], using Glen's flow with flow exponent $n = 3$ and a nonlinear Weertman-type sliding law with sliding exponent $m = 3$. The model employs finite element methods on an unstructured mesh with six-node elements and quadratic base functions. The maximum distance between triangle vertices is 2 km over the ice shelf and less than 0.5 km in both the vicinity of the grounding line and the deep glacier valleys. An estimate of model uncertainties related to mesh resolution are given in the supporting information. All observational data sets were mapped onto the model grid using linear interpolation. As the region is topographically complex, rock outcrops were outlined using Landsat imagery, which greatly improved the accuracy compared to outlines available from the SCAR Antarctic Digital Database 6.0 (www.add.scar.org). Outcrops and nunataks were treated as holes in the mesh, and no-normal flow conditions for the ice were imposed along their boundaries. At the ice divide on the Bruce Plateau, obtained from *Cook et al.* [2014], a zero velocity condition was imposed.

We employed the inversion capabilities of Úa to minimize the mismatch between modeled (u_{mod}) and observed (u_{obs}) surface velocities. Following techniques for adjoint optimization in glaciology first introduced

by *MacAyeal* [1992, 1993] and now commonly used, the control parameters in the inversion are the basal slipperiness C, and the rate factor A. Both parameters were updated consecutively with every increment in C followed by an increment in A, for a total of 50 iterations, leading to a mean difference between modeled and observed surface velocities of 26.4 m a^{-1} with a spread of 42 m a^{-1} (see Figure S1 in the supporting information). For fast-flowing areas with $u_{obs} > 100$ m a^{-1}, the mean relative error between the model and observations is 13.6%.

Adjoint methods have been used perviously to obtain information about the rheology of the LBIS before its disintegration [*Vieli et al.*, 2006; *Khazendar et al.*, 2007; *Borstad et al.*, 2012], but an inversion for both slipperiness and rheology of the region, including the tributary glaciers, has not been attempted before. Our analysis simulates the important flow features with high surface velocities in the valleys and close-to-stagnant ice on the steep slopes and toward the Bruce Plateau. The model fails to resolve the sharp gradient in velocities along the Seal Nunataks, as well as the narrow (∼1 grid cell) shear margin of Crane Glacier (see Figure S1). Larger than average errors in the surface velocities are also found close to the grounding line. The shear margins along the Jason Peninsula in the south and along other valley side walls are well reproduced.

The resulting basal slipperiness varies over several orders of magnitude with $C \in [10^{-5}, 10^{-2}]$ m a^{-1} kPa^{-3}, with a generally increasing trend toward the grounding line and no significant variations at spatial scales on the order of a few ice thicknesses. The rate factor, A, reveals regions of soft ice along the margins ($A \sim 2 \times 10^{-8}$ a^{-1} kPa^{-3}), which correspond to areas of increased shear (south of the Seal Nunataks) or with a highly crevassed surface (around Cape Disappointment). Regions of stiffer ice ($A \sim 2 \times 10^{-9}$ a^{-1} kPa^{-3}) are found in the interior of the ice shelf, in particular, downstream of the outflow regions of Crane, Leppard and Flask Glaciers, which could be associated with the outflow of colder ice from those regions. Our simulations produce a rheology pattern and values that are broadly similar to previously obtained results using different data sets and methods [*Khazendar et al.*, 2007]. More details are given in Figure S2.

4. Ice Shelf Buttressing

Recent studies have solved the stress balance of coupled ice stream-ice shelf systems in both horizontal dimensions [*Goldberg et al.*, 2009; *Katz and Worster*, 2010; *Gudmundsson*, 2013; *Favier et al.*, 2014], showing a complicated stress pattern for confined ice shelves. At the grounding line, the pattern provides a total resistive force that affects the seaward motion of the grounded ice. This so-called ice shelf buttressing is a mechanism that inherently operates in two horizontal dimensions and is the combined result of shear stresses at the ice shelf margin, the basal resistance at local pinning points, and the bending stresses at the ice front. These effects cannot be captured adequately by flow line models for complicated geometries like the LBIS, and the use of a model that resolves both horizontal dimensions at sufficiently fine resolution is therefore essential.

A convenient measure for the local amount of buttressing at the grounding line, σ_b, is the difference between the ocean pressure that would act normal to the grounding line in the absence of the ice shelf (denoted by N_0) and the actual normal pressure in the presence of the ice shelf (denoted by N) [*Gudmundsson*, 2013]

$$\begin{aligned} \sigma_b &= N_0 - N \\ &= \frac{1}{2}\varrho g h - \hat{\boldsymbol{n}}_{\mathrm{gl}}^T \cdot \left(\boldsymbol{R}\hat{\boldsymbol{n}}_{\mathrm{gl}}\right) , \end{aligned} \tag{1}$$

where h is the ice thickness, g the gravitational acceleration, and $\varrho = \rho_i \left(1 - \frac{\rho_i}{\rho_w}\right)$ with $\rho_i = 918$ kg m^{-3} and $\rho_w = 1028$ kg m^{-3} the ice and ocean densities, respectively. The vector $\hat{\boldsymbol{n}}_{\mathrm{gl}}$ is the unit normal to the grounding line, and

$$\boldsymbol{R} = \begin{pmatrix} 2\tau_{xx} + \tau_{yy} & \tau_{xy} \\ \tau_{xy} & 2\tau_{yy} + \tau_{xx} \end{pmatrix} \tag{2}$$

with τ_{ij} the components of the deviatoric stress tensor. Negative values for σ_b indicate areas where the ice shelf pulls the ice outward and away from the grounding line, whereas positive values indicate a net resistive force, which restricts the motion of grounded ice.

Model results for σ_b along the 1995 grounding line of the LBIS are plotted as a band parallel to the grounding line in Figure 2a. Results are positive everywhere, except for a small region south of Evans Glacier, at the grounding line of Pequod Glacier, and around Cape Disappointment. Values range from $\sigma_b = -10$ kPa to

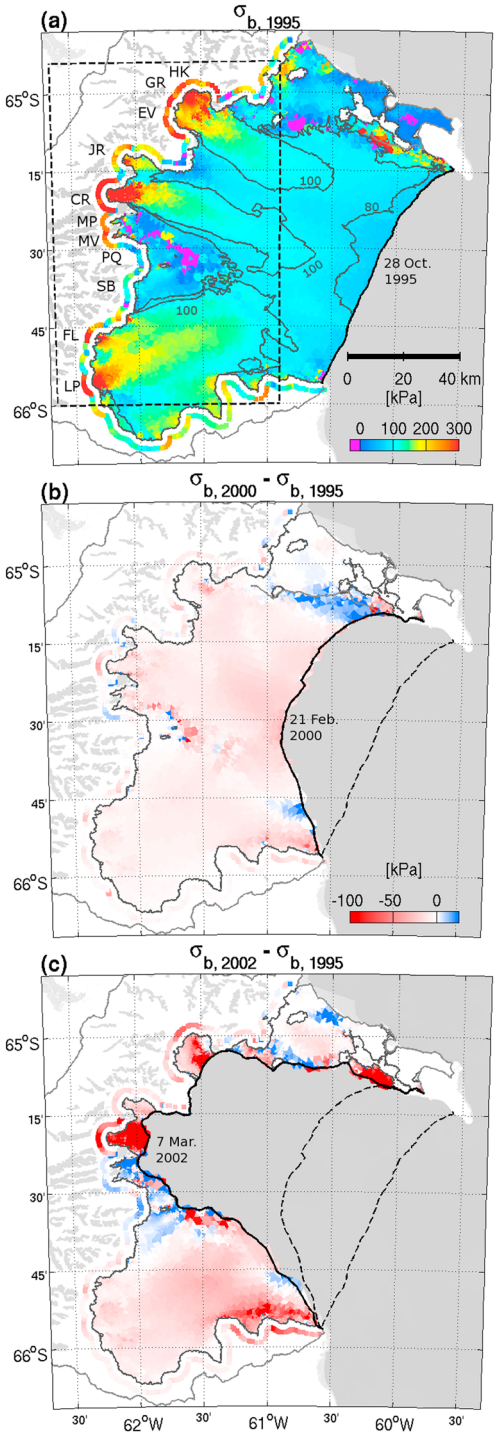

Figure 2. (a) Model results for the backstress σ_b in 1995. The narrow band plotted parallel to the grounding line shows values of σ_b as obtained from equation (1). Values on the ice shelf are defined in a similar way, but with $\hat{\boldsymbol{n}}_{gl}$ (unit normal to the grounding line) replaced by $\hat{\boldsymbol{e}}_u$ (unit vector along the flow). Black lines on the ice shelf highlight the $\sigma_b = 80$ kPa and $\sigma_b = 100$ kPa contours. Names of the outlet glaciers are indicated by their acronym, as in Figure 1. The dashed rectangle delineates the spatial extent of Figure 3. (b) Instantaneous change in backstress compared to 1995 for the new ice front position on 21 February 2000. (c) Same as in Figure 2b but for the ice front position immediately after the collapse on 7 March 2002.

about $\sigma_b = 400$ kPa, in agreement with values found in the literature [*Thomas and McAyeal*, 1982; *Borstad et al.*, 2013] and with the highest backstress obtained in areas where the tributary glaciers flow into the ice shelf.

In order to understand the propagation of backstress through the ice shelf, it is convenient to replace $\hat{\boldsymbol{n}}_{gl}$ in equation (1) by $\hat{\boldsymbol{e}}_u$, a unit vector parallel to the local flow direction. The resulting quantity can be interpreted as the difference between the buoyancy-driven along-flow stress, which the ice shelf would experience if it was unconfined and the net along-flow stress [*Thomas*, 1973]. The results are plotted on the same color scale in Figure 2a. The backstress in the ice shelf generally decreases from $\sigma_b > 300$ kPa in the outflow regions of the main tributary glaciers, to $\sigma_b < 100$ kPa toward the ice front. Low values are also found in areas of relatively stagnant ice around the Seal Nunataks, Foyn Point, and Cape Disappointment. The smaller, slow-flowing glaciers that feed these areas experience a reduced backstress: Jorum ($\sigma_b < 250$ kPa), Mapple and Melville ($\sigma_b < 300$ kPa), and Pequod and Starbuck Glaciers ($\sigma_b < 150$ kPa).

5. Response of Glaciers to Ice Shelf Collapse

A reduction in buttressing over time ($d\sigma_b/dt < 0$) occurs when the ice shelf thins and weakens through surface or basal processes, or when its extent decreases through calving or disintegration. In the case of the LBIS, the loss of 2289 km^2 of the ice shelf between October 1997 and February 2000 through a series of calving events and the collapse of 3292 km^2, or a further 40% over the course of a few weeks in February 2002, led to a large perturbation in stresses at the grounding line.

We study the *instantaneous* change in the backstress imposed by the ice shelf and the associated change in ice flow velocity, as a response to an instantaneous retreat of the ice front. The (time-independent) diagnostic equations were solved for the new ice front position, keeping all other model parameters (including basal

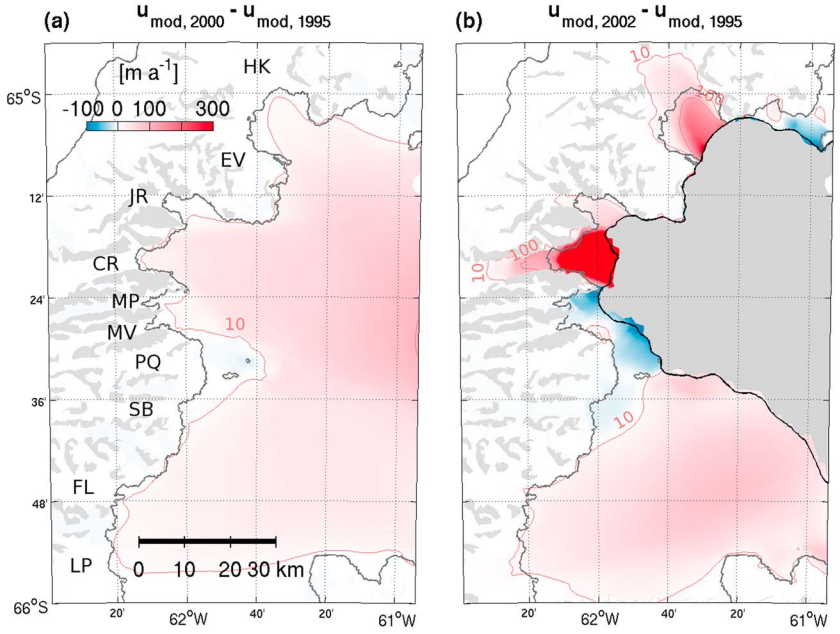

Figure 3. Absolute change in model velocities compared to 1995 for new ice front positions on (a) 21 February 2000 and (b) 7 March 2002. Red lines are the 10 m a^{-1} and 100 m a^{-1} change in velocity contours.

slipperiness, ice viscosity, ice thickness, and grounding line position) constant. We consider two new ice front locations: (a) the location for 21 February 2000, 2 years before the breakup and (b) the location for 7 March 2002, just after the breakup. The instantaneous change in backstress compared to 1995 for each of the new ice-front positions is shown in Figures 2b and 2c. Between 1995 and 2000, calving caused an average change in backstress at the grounding line of $< \sigma_{b,2000} - \sigma_{b,1995} > = -5$ kPa with a spread of 10 kPa, while σ_b decreased uniformly across most of the ice shelf by a similar amount. The tributary glaciers experienced a limited reduction in buttressing on the order of a few percent, with the largest change at the grounding line of Crane Glacier (−10%).

The rapid disintegration of the central part of the ice shelf in 2002 caused a much larger and spatially more complex perturbation in the backstress (Figure 2c). At the grounding line of Crane Glacier, σ_b decreased by up to 100 kPa or 30%. For Hectoria and Green Glaciers, the reduction was somewhat smaller (−60 kPa) but still accounted for a loss of up to 20% of the original buttressing. The backstress across the remnant Scar Inlet generally decreased, in particular, along its southeastern margin, though σ_b at the grounding line remained largely unaltered compared to 1995. Interestingly, and in contrast to other areas, the backstress for the small glaciers south of Crane Glacier remained largely unchanged (Mapple and Pequod) or increased slightly (Melville, +10 kPa or +5%).

The instantaneous change in buttressing directly affects the flow, as the ice readjusts to the new stress conditions at its boundaries. In equation (1), the ice thickness h stays constant, and the change in backstress is entirely due to changes in the deviatoric stresses. The latter are related to the velocities via a nonlinear flow law, which leads to a nontrivial relationship between changes in σ_b and changes in u_{mod}. In Figure 3, we show the difference between modeled surface velocities in (a) 2000 and 1995 and (b) 2002 and 1995, for an area around the grounding line which includes all major tributary glaciers and a large part of Scar Inlet.

For the 2000 ice front, changes are small (+10%) and limited to the ice shelf. However, nonlocal effects can play an important role in transmitting the perturbation in buttressing upstream of the grounding line. Figure 3b shows that after the collapse of the ice shelf in 2002, instantaneous changes in surface velocity larger than 5% are found over the first 15 km upstream from the grounding line of Hektoria, Green, and Crane Glaciers. In agreement with changes in the backstress, the response to the collapse of the ice shelf is regionally diverse, with a widespread increase in speed for Hektoria, Green, Jorum, and Crane Glaciers, a smaller speedup of Scar

Inlet but a limited response of its tributary glaciers (Flask and Leppard), and a little or no change in surface speed for the narrow glaciers south of Crane Glacier (Pequod, Mapple, Melville).

6. Discussion

Despite signs of mechanical weakening of the ice shelf prior to its collapse [*Rack et al.*, 2000], the dominant loss of buttressing for the tributary glaciers was near-instantaneous, as the main part of the ice shelf broke away over the course of a few weeks in February 2002. This justifies the application of an instantaneous ice front perturbation in the model. The earliest observations of glacier velocities after the collapse date from December 2003, i.e., less than 2 years after the event [*Wuite et al.*, 2015]. During this period, Hektoria and Green Glaciers increased their center line speed from about 365 m a^{-1} at the 1995 grounding line to more than 2000 m a^{-1} (or a sixfold increase) in 2003, while the grounding line retreated by several kilometers. These observations show that the response to the perturbation was immediate and large in amplitude.

When Figure 3b is compared to Figure 1 (note the difference in color scale), obvious similarities are apparent between the modeled velocity changes and observations. The three main outlets (Hektoria-Green, Jorum, and Crane Glaciers) show the largest speedup in both cases. However, despite a clear speedup of Evans Glacier in the long-term observational record, no such response is evident from the instantaneous change in modeled velocities.

A smaller increase in surface velocities is modeled for Scar Inlet, and little change is seen for its tributary glaciers (Starbuck, Leppard, and Flask). This corresponds well to observations of an immediate impact on the stress field through rift formation and acceleration of Scar Inlet, and a smaller and delayed signal in observed surface velocities for its tributary glaciers [*Wuite et al.*, 2015]. The work of *Khazendar et al.* [2015] has shown that the limited response of Leppard and Flask Glaciers is likely related to a reduction in buttressing by the Scar Inlet. Finally, the modeled velocities for the narrow glaciers south of Crane Glacier (Mapple, Melville, and Pequod) remain unchanged, which is also reflected in the observational record. No statistically significant change in velocities or frontal position has been observed to date for Mapple and Pequod, whereas Melville has only shown a local twofold speedup near its ice front between 1995 and 2007, which is likely related to a further retreat of its frontal position by about 2 km since 2002 [*Wuite et al.*, 2015].

The net result of the ice shelf collapse is an instantaneous increase of modeled mass flux across the grounding line by 1.17 Gt a^{-1}: from a total flux of 11.50 Gt a^{-1} in 1995, to a net flux of 12.67 Gt a^{-1} immediately after the collapse. This modeled increase is almost an order of magnitude smaller than the estimated mass loss of 8 Gt a^{-1} from observations between 2001 and 2008 by *Scambos et al.* [2014] and comparable results by *Wuite et al.* [2015]. As our model experiment is intended to simulate instantaneous changes, and numbers reported by *Scambos et al.* [2014] and *Wuite et al.* [2015] refer to different dates and a longer time frame, a match between our results and these observations cannot be expected. Likely explanations for the difference are (a) a further reduction in backstress as the ice front continued to retreat rapidly within the months and years after the collapse [*Rack and Rott*, 2004], as can be seen from the ice front position in 2009 in Figure 1 and (b) the importance of transient effects, i.e., the evolution of ice thickness and velocity over time, as well as feedback mechanisms related to grounding line movement and possible changes to basal slipperiness and ice viscosity.

Such variations have been discarded in this study, and future transient model experiments are required to obtain a match with long-term observations from *Scambos et al.* [2014] and *Wuite et al.* [2015]. As a first approximation, a diagnostic perturbation experiment can be performed in which the ice front is moved to a more recent location, keeping the ice thickness and other model parameters equal to their pre-ice-shelf collapse values. Similar to experiments presented in section 5, the instantaneous change in backstress and velocities for the individual catchments can be monitored and compared to precollapse values. An example of such an experiment for the ice front location on 20 February 2009 is discussed in the supporting information.

7. Conclusions

Modeling the regionally diverse response of glaciers following the collapse of the Larsen B Ice Shelf is challenging and has not been attempted before. In this study, a state-of-the-art ice shelf-ice sheet model was used to invert for the precollapse englacial and basal properties of the area, using a recently obtained and complete data set of surface velocities and ice thickness. The model performs well in replicating the ice flow

conditions prior to the collapse of the ice shelf and provides new insights into the spatial distribution of backforces imposed by the ice shelf. Results from a number of perturbation experiments were presented which demonstrate the complex behavior of backstresses and surface velocities immediately after the collapse of the ice shelf. A reduction in back pressure up to 30% was shown for the main tributary glaciers. The diagnostic model experiments could accurately reproduce the spatial variability of the response, though transient effects were found to be essential to reproduce the quantitative changes that have been observed since the collapse.

Acknowledgments

We thank Stephen Cornford and Daniel Farinotti for their helpful comments and suggestions. J.D.R. was funded through a Marie Curie fellowship (European Union Seventh Framework Programme (FP7/2007–2013), grant PIEF-GA-2011-301268), and J.D.R. and G.H.G. were partly supported by core funding from the Natural Environment Research Council (NERC) to the British Antarctic Survey. J.L.B. was partly funded by NERC grant NE/I027401/1.

The Editor thanks Daniel Farinotti and an anonymous reviewer for their assistance in evaluating this paper.

References

Barrand, N. E., et al. (2013), Computing the volume response of the Antarctic Peninsula ice sheet to warming scenarios to 2200, *J. Glaciol.*, *59*(215), 397–409.

Berthier, E., T. A. Scambos, and C. A. Shuman (2012), Mass loss of Larsen B tributary glaciers (Antarctic Peninsula) unabated since 2002, *Geophys. Res. Lett.*, *39*, L13501, doi:10.1029/2012GL051755.

Borstad, C. P., A. Khazendar, E. Larour, M. Morlighem, E. Rignot, M. P. Schodlok, and H. Seroussi (2012), A damage mechanics assessment of the Larsen B ice shelf prior to collapse: Toward a physically-based calving law, *Geophys. Res. Lett.*, *39*, L18502, doi:10.1029/2012GL053317.

Borstad, C. P., E. Rignot, J. Mouginot, and M. P. Schodlok (2013), Creep deformation and buttressing capacity of damaged ice shelves: Theory and application to Larsen C ice shelf, *Cryosphere*, *7*(6), 1931–1947.

Cook, A., D. Vaughan, A. Luckman, and T. Murray (2014), A new Antarctic Peninsula glacier basin inventory and observed area changes since the 1940s, *Antarct. Sci.*, *26*(06), 614–624.

Cook, A. J., and D. G. Vaughan (2010), Overview of areal changes of the ice shelves on the Antarctic Peninsula over the past 50 years, *Cryosphere*, *4*(1), 77–98.

Cook, A. J., T. Murray, A. Luckman, D. Vaughan, and N. Barrand (2012), A new 100-m digital elevation model of the Antarctic Peninsula derived from ASTER Global DEM: Methods and accuracy assessment, *Earth Syst. Sci. Data*, *4*, 129–142.

Favier, L., G. Durand, S. Cornford, G. Gudmundsson, O. Gagliardini, F. Gillet-Chaulet, T. Zwinger, A. Payne, and A. Le Brocq (2014), Retreat of Pine Island Glacier controlled by marine ice-sheet instability, *Nat. Clim. Change*, *4*(2), 117–121.

Fretwell, P., et al. (2013), Bedmap2: Improved ice bed, surface and thickness datasets for Antarctica, *Cryosphere*, *7*(1), 375–393.

Goldberg, D., D. M. Holland, and C. Schoof (2009), Grounding line movement and ice shelf buttressing in marine ice sheets, *J. Geophys. Res.*, *114*, F04026, doi:10.1029/2008JF001227.

Gudmundsson, G. H. (2013), Ice-shelf buttressing and the stability of marine ice sheets, *Cryosphere*, *7*(2), 647–655.

Gudmundsson, G. H., J. Krug, G. Durand, L. Favier, and O. Gagliardini (2012), The stability of grounding lines on retrograde slopes, *Cryosphere*, *6*(6), 1497–1505.

Hindmarsh, R. C., and E. Le Meur (2001), Dynamical processes involved in the retreat of marine ice sheets, *J. Glaciol.*, *47*(157), 271–282.

Holland, P. R., H. F. J. Corr, D. G. Vaughan, A. Jenkins, and P. Skvarca (2009), Marine ice in Larsen Ice Shelf, *Geophys. Res. Lett.*, *36*, L11604, doi:10.1029/2009GL038162.

Holland, P. R., H. F. J. Corr, H. D. Pritchard, D. G. Vaughan, R. J. Arthern, A. Jenkins, and M. Tedesco (2011), The air content of Larsen Ice Shelf, *Geophys. Res. Lett.*, *38*, L10503, doi:10.1029/2011GL047245.

Hulbe, C. L., T. A. Scambos, T. Youngberg, and A. K. Lamb (2008), Patterns of glacier response to disintegration of the Larsen B ice shelf, Antarctic Peninsula, *Global Planet. Change*, *63*(1), 1–8.

Huss, M., and D. Farinotti (2014), A high-resolution bedrock map for the Antarctic Peninsula, *Cryosphere*, *8*(4), 1261–1273.

Hutter, K. (1983), *Theoretical Glaciology: Material Science of Ice and the Mechanics of Glaciers and Ice Sheets*, Mathematical Approaches to Geophysics, Springer, Netherlands.

Katz, R. F., and M. G. Worster (2010), Stability of ice-sheet grounding lines, *Proc. R. Soc. A*, *466*, 1597–1620.

Khazendar, A., E. Rignot, and E. Larour (2007), Larsen B ice shelf rheology preceding its disintegration inferred by a control method, *Geophys. Res. Lett.*, *34*, L19503, doi:10.1029/2007GL030980.

Khazendar, A., C. P. Borstad, B. Scheuchl, E. Rignot, and H. Seroussi (2015), The evolving instability of the remnant Larsen B Ice Shelf and its tributary glaciers, *Earth Planet. Sci. Lett.*, *419*, 199–210.

Kulessa, B., D. Jansen, A. J. Luckman, E. C. King, and P. R. Sammonds (2014), Marine ice regulates the future stability of a large Antarctic ice shelf, *Nat. Commun.*, *5*, 3707, doi:10.1038/ncomms4707.

MacAyeal, D. R. (1989), Large-scale ice flow over a viscous basal sediment: Theory and application to ice stream B, Antarctica, *J. Geophys. Res.*, *94*(B4), 4071–4087.

MacAyeal, D. R. (1992), The basal stress distribution of Ice Stream E, Antarctica, inferred by control methods, *J. Geophys. Res.*, *97*(B1), 595–603.

MacAyeal, D. R. (1993), A tutorial on the use of control methods in ice-sheet modeling, *J. Glaciol.*, *39*(131), 91–98.

Padman, L., H. A. Fricker, R. Coleman, S. Howard, and L. Erofeeva (2002), A new tide model for the Antarctic ice shelves and seas, *Ann. Glaciol.*, *34*(1), 247–254.

Pattyn, F., et al. (2012), Results of the Marine Ice Sheet Model Intercomparison Project, MISMIP, *Cryosphere*, *6*(3), 573–588.

Pattyn, F., et al. (2013), Grounding-line migration in plan-view marine ice-sheet models: Results of the ice2sea MISMIP3d intercomparison, *J. Glaciol.*, *59*(215), 410–422.

Pritchard, H., S. Ligtenberg, H. Fricker, D. Vaughan, M. van den Broeke, and L. Padman (2012), Antarctic ice-sheet loss driven by basal melting of ice shelves, *Nature*, *484*(7395), 502–505.

Rack, W., and H. Rott (2004), Pattern of retreat and disintegration of the Larsen B ice shelf, Antarctic Peninsula, *Ann. Glaciol.*, *39*(1), 505–510.

Rack, W., C. S. Doake, H. Rott, A. Siegel, and P. Skvarca (2000), Interferometric analysis of the deformation pattern of the northern Larsen Ice Shelf, Antarctic Peninsula, compared to field measurements and numerical modeling, *Ann. Glaciol.*, *31*(1), 205–210.

Rebesco, M., et al. (2014), Boundary condition of grounding lines prior to collapse, Larsen-B Ice Shelf, Antarctica, *Science*, *345*(6202), 1354–1358.

Rignot, E., G. Casassa, P. Gogineni, W. Krabill, A. Rivera, and R. Thomas (2004), Accelerated ice discharge from the Antarctic Peninsula following the collapse of Larsen B ice shelf, *Geophys. Res. Lett.*, *31*, L18401, doi:10.1029/2004GL020697.

Ritz, C., V. Rommelaere, and C. Dumas (2001), Modeling the evolution of Antarctic ice sheet over the last 420,000 years: Implications for altitude changes in the Vostok region, *J. Geophys. Res.*, *106*(D23), 31,943–31,964.

Rott, H., P. Skvarca, and T. Nagler (1996), Rapid collapse of Northern Larsen ice shelf, Antarctica, *Science*, *271*(5250), 788–792.

Rott, H., W. Rack, P. Skvarca, and H. De Angelis (2002), Northern Larsen ice shelf, Antarctica: Further retreat after collapse, *Ann. Glaciol.*, *34*(1), 277–282.

Rott, H., F. Müller, T. Nagler, and D. Floricioiu (2011), The imbalance of glaciers after disintegration of Larsen-B ice shelf, Antarctic Peninsula, *Cryosphere*, *5*(1), 125–134.

Scambos, T. A., C. Hulbe, M. Fahnestock, and J. Bohlander (2000), The link between climate warming and break-up of ice shelves in the Antarctic Peninsula, *J. Glaciol.*, *46*(154), 516–530.

Scambos, T. A., J. A. Bohlander, C. A. Shuman, and P. Skvarca (2004), Glacier acceleration and thinning after ice shelf collapse in the Larsen B embayment, Antarctica, *Geophys. Res. Lett.*, *31*, L18402, doi:10.1029/2004GL020670.

Scambos, T. A., E. Berthier, and C. A. Shuman (2011), The triggering of subglacial lake drainage during rapid glacier drawdown: Crane Glacier, Antarctic Peninsula, *Ann. Glaciol.*, *52*(59), 74–82.

Scambos, T. A., E. Berthier, T. Haran, C. A. Shuman, A. J. Cook, S. R. M. Ligtenberg, and J. Bohlander (2014), Detailed ice loss pattern in the northern Antarctic Peninsula: Widespread decline driven by ice front retreats, *Cryosphere*, *8*(6), 2135–2145.

Shuman, C. A., E. Berthier, and T. A. Scambos (2011), 2001–2009 elevation and mass losses in the Larsen A and B embayments, Antarctic Peninsula, *J. Glaciol.*, *57*(204), 737–754.

Thomas, R. H. (1973), The creep of ice shelves: Theory, *J. Glaciol.*, *12*, 45–53.

Thomas, R. H., and D. R. McAyeal (1982), Derived characteristics of the Ross Ice Shelf, Antarctica, *J. Glaciol.*, *28*, 397–412.

Vieli, A., and A. J. Payne (2005), Assessing the ability of numerical ice sheet models to simulate grounding line migration, *J. Geophys. Res.*, *110*, F01003, doi:10.1029/2004JF000202.

Vieli, A., A. J. Payne, Z. Du, and A. Shepherd (2006), Numerical modelling and data assimilation of the Larsen B ice shelf, Antarctic Peninsula, *Philos. Trans. R. Soc. A*, *364*(1844), 1815–1839.

Vieli, A., A. Payne, A. Shepherd, and Z. Du (2007), Causes of pre-collapse changes of the Larsen B ice shelf: Numerical modelling and assimilation of satellite observations, *Earth Planet. Sci. Lett.*, *259*(3–4), 297–306.

Wouters, B., A. Martin-Espanol, V. Helm, T. Flament, J. van Wessem, S. Ligtenberg, M. van den Broeke, and J. Bamber (2015), Dynamic thinning of glaciers on the Southern Antarctic Peninsula, *Science*, *348*(6237), 899–903.

Wuite, J., H. Rott, M. Hetzenecker, D. Floricioiu, J. De Rydt, G. H. Gudmundsson, T. Nagler, and M. Kern (2015), Evolution of surface velocities and ice discharge of Larsen B outlet glaciers from 1995 to 2013, *Cryosphere*, *9*, 957–969.